Biosensors and Bioelectronics 26 (2011) 2967–2974

Contents lists available at ScienceDirect

Biosensors and Bioelectronics

journal homepage: www.elsevier.com/locate/bios

Chitosan–iron oxide nano-composite platform for mismatch-discriminating DNA hybridization for *Neisseria gonorrhoeae* detection causing sexually transmitted disease

Renu Singh[a,c], Rachna Verma[b], Ajeet Kaushik[a], Gajjala Sumana[a], Seema Sood[b], Rajinder K. Gupta[c], B.D. Malhotra[a,*]

[a] DST Centre on Biomolecular Electronics, Biomedical Instrumentation Section, National Physical Laboratory (CSIR), Dr. K.S. Krishnan Marg, New Delhi 110012, India
[b] Department of Microbiology, All India Institute of Medical Sciences, New Delhi 110002, India
[c] School of Biotechnology, Guru Gobind Singh Indraprastha University, Kashmere Gate, Delhi 110006, India

ARTICLE INFO

Article history:
Received 17 August 2010
Received in revised form 1 November 2010
Accepted 29 November 2010
Available online 7 December 2010

Keywords:
Neisseria gonorrhoeae
Sexually transmitted disease
Chitosan–Fe_3O_4 nanostructure
Methylene blue
Electrochemical sensor

ABSTRACT

Electrochemically fabricated nano-composite film of chitosan (CH)–iron oxide (Fe_3O_4) has been used to detect gonorrhoea, a sexually transmitted disease (STD) via immobilization of biotinylated probe DNA (BDNA) using avidin–biotin coupling for rapid and specific (mismatch-discriminating) DNA hybridization. The presence of Fe_3O_4 nanoparticles (~18 nm) increases the electro-active surface area of the nano-biocomposite that provides desirable environment for loading of DNA with better conformation leading to increased electron transfer kinetics between the medium and electrode. The differential pulse voltammetric (DPV) studies have been conducted using BDNA/avidin/CH–Fe_3O_4/ITO electrode owing to the reduction of the methylene blue (MB) indicator and investigate electron transfer between MB moieties and electrode for one and two-bases mismatch. This STD biosensor is found to have a detection limit (1×10^{-15} M) and a wide dynamic range (from 1×10^{-16} M to 1×10^{-6} M) using the complementary target DNA. In addition, the sensing system can be utilized to accurately discriminate complementary sequence from mismatch sequences.

1. Introduction

Gonorrhoea is a bacterial sexually transmitted infection (STI) caused by *Neisseria gonorrhoeae* (Whitehead et al., 2007). Global estimates indicate that 62 million infections occur each year attesting to its public health importance. Current incidence figures indicate that it is the highest in 53 years (WHO, 2001). Due to the limitations of the conventional methods of diagnosis; i.e., microscopy and culture, in terms of sensitivity and specificity especially in the case of female patients (Mukenge-Tshibaka et al., 2000), the increased use of molecular methods is being widely advocated. Polymerase chain reaction (PCR) has been the most widely used amplification method and is being carried out in various laboratories worldwide for the diagnosis of gonorrhoea. A sensitivity of up to 100% and a specificity of up to 99.5% can be obtained using PCR, depending upon the gene being amplified and the target population in which the PCR has been evaluated. However, the sensitivity decreases considerably in urine samples resulting up to 50% false negatives (Smith et al., 2005). Fabrication of a DNA based biosensor for the detection of *N. gonorrhoeae* may provide an alternative diagnostic methodology may be used to examine patients using non-invasive self-collected specimen, e.g., urine and at the same time may aid in identifying asymptomatic patients due to its high sensitivity. In this context, the specificity of any diagnostic test for *N. gonorrhoeae* is a very critical parameter as it has a 93% homology with *Neisseria meningitidis* at DNA level (Tabrizi et al., 2004). Also, the gonococcus has a well-developed capacity for genetic variation and recombination making cross-reaction with commensal *Neisseria* sp. a common phenomenon. The present study has been carried out to evaluate the biotinylated probe DNA in terms of its mismatch-discriminating capacity using a panel of oligonucleotide sequences with mismatches introduced at different positions.

Metal nanoparticles and conducting polymers are playing an important role in the fabrication of nanodevices for the diagnosis of the infectious diseases (Peppas et al., 2006) because of their unique properties like large surface-to-volume ratio, high surface reaction activity, high catalytic efficiency, strong adsorption ability, particle size, electrical properties, and surface properties (Iida et al., 2007) that are helpful for the immobilization of biomolecules. One of the major discoveries in the application of nanoparticles

* Corresponding author. Tel.: +91 11 45609152.
E-mail address: bansi.malhotra@gmail.com (B.D. Malhotra).

0956-5663/$ – see front matter © 2010 Elsevier B.V. All rights reserved.
doi:10.1016/j.bios.2010.11.047

relates to the realization of the steric stabilization that may increase the nano-particle stability in the biological environment for the application to biosensing. In this context, Fe_3O_4 nanoparticles have been found to play distinct roles in chemical, medical and industrial fields (Gong et al., 2007) because of their interesting magnetic properties, biocompatibility, and potential applications in the field of clinical diagnostics (Guo et al., 2007) and sensors (Katz et al., 2005). However, their tendency to aggregate limits their biosensing applications. Dispersing Fe_3O_4 in a suitable matrix like chitosan to prevent aggregation is an interesting alternative. Now-a-days, several techniques have been developed to fabricate Fe_3O_4 films (Loh et al., 2008), including sputtering (Tripathy and Adeyeye, 2005), dip coating (Cao et al., 2003), Langmuir–Blodgett deposition (Lee et al., 2007) and layer-by-layer electrochemical deposition (Huang et al., 2004). Among these, electrochemical technique has attracted much interest for the fabrication of matrix because of simplicity, easy controllability to tailor desired properties with the advantage of uniformity.

The electrochemical approach for the synthesis of CH/Fe_3O_4 nanostructured composite onto ITO substrate, without using a template, catalyst, or surfactant is considered to be a facile method. It is known that CH is an interesting material with both strong inter- and intra-molecular hydrogen bonding interactions due to presence of the hydroxyl and amino groups. And with these functional groups, CH has an intrinsically strong affinity to many different types of biological substances. In our approach, the subtle variations of hydrogen-bonding interactions under the applied electric field are expected to act as driving force to direct anisotropic growth of CH nanostructure along with Fe_3O_4 nanoparticles. It has been demonstrated that nanoscale morphology of CH can be adjusted by tuning reaction conditions during electrochemical synthesis.

We report results of studies relating to fabrication of CH–Fe_3O_4/ITO nano-biocompatible composite for the detection of *N. gonorrhoeae* using DNA hybridization technique. Detection of nucleotide mismatches using an electrochemical approach offers benefits of an ultrasensitive detection method without any prior labeling and signal-amplification procedure. Keeping this in view, we attempt to fabricate an electrochemical sensor for the detection of *N. gonorrhoeae* and systematically analyse mismatch-discriminating DNA hybridization.

2. Experimental

2.1. Chemicals and reagents

Chitosan, methylene blue (MB), tris base, ethylene diamine tetra acetic acid (EDTA), potassium monohydrogen phosphate, potassium dihydrogen phosphate, iron-oxide (Fe_3O_4) nanoparticles and avidin (Avi) have been procured from Sigma–Aldrich, USA. Indium-tin-oxide (ITO) coated glass plates (0.25 cm^2) have been obtained from Balzers, UK. All other chemicals are of analytical grade. Deionized water (resistance ~18.2 MΩ) from the Millipore water purification system has been utilized for preparation of the desired aqueous solutions. All the solutions and glassware are autoclaved prior to being used.

2.2. Synthesis of DNA sequences

Oligonucleotide probe sequence for specific detection of *N. gonorrhoeae* has been identified from the *opa* gene (a multi-copy gene) of *N. gonorrhoeae*. All oligonucleotide sequences have been procured from Sigma–Aldrich, USA. The oligonucleotide sequences, matched and mismatched duplex DNA used for immobilization in this study are shown in Tables 1a and 1b. Probe: BDNA or biotin (GenBank accession no: PUID 9716119 snum 2705).

Table 1a
Oligonucleotide sequences used for immobilization.

S. no.	Oligonucleotide	Sequence
1.	Probe DNA: biotin (BDNA)	5′-CCGGTGCTTCATCACCTTAG-3′
2.	Complementary target DNA (cDNA)	5′-CTAAGGTGATGAAGCACCGG-3′
3.	One-base mismatch DNA (OBM1)	5′-CTAAGTTGATGAAGCACCGG-3′
4.	One-base mismatch DNA (OBM2)	5′-CTAAGGTGACGAAGCACCGG-3′
5.	Two-base mismatch DNA (TBM1)	5′-CTAAGTTGATGAAACACCGG-3′
6.	Two-base mismatch DNA (TBM2)	5′-CTAGGGTGACGAAGCACCGG-3′
7.	Two-base mismatch DNA (TBM3)	5′-CTAAGTTGACGAAGCACCGG-3′

2.3. Electrochemical deposition of CH–Fe_3O_4 onto ITO electrode

Chitosan (0.50%) solution is prepared by dissolving CH (50 mg) in 10 mL of acetate buffer (0.05 M, pH 4.2) and is kept for 4 days to obtain a clear solution at 25 °C. 5 mg of Fe_3O_4 nanoparticles is dispersed in CH solution by stirring at room temperature after which it is sonicated for about 10 h. Finally, a highly viscous solution of CH with uniformly dispersed Fe_3O_4 nanoparticles (characterized by X-ray diffraction (XRD), vibrating sample magnetometeric (VSM), please see Supplementary fig. 1a,b) is obtained and used for electrochemical deposition. CH and Fe_3O_4 nanoparticles have been taken as 10:1 to prepare CH–Fe_3O_4/ITO nano-composite film which exhibits maximum electrochemical current response (Kaushik et al., 2008). CH–Fe_3O_4/ITO nano-composite films are prepared onto ITO plate (0.25 cm^2) using the electrochemical deposition of quiescent solution of CH–Fe_3O_4. ITO substrates are chosen because it is known that an oxide surface can interact strongly with –OH and $-NH_2$ of CH (Li et al., 2005). The ITO plates are precleaned with acetone, ethanol, and a copious amount of deionized water. To obtain uniform distribution of OH group on ITO surface, ITO plates are immersed in a solution of H_2O_2/NH_4OH/H_2O (1:1:5, v/v) for 30 min at 80 °C for hydrolysis, after which they are rinsed thoroughly with deionized water and dried. The deposition is performed chrono-amperometrically at −1.0 V for 360 s (via intermittent washing using autoclaved Millipore water after every 120 s of deposition). Then, the electrode is rinsed with autoclaved Millipore water three times to remove any unbound particles and then air-dried. In this way, a robust and highly ordered CH–Fe_3O_4/ITO nano-composite is obtained. In addition, in a separate experiment, when CH solution is drop-cast onto a substrate (which is equivalent to a deposition at zero potential), only featureless CH particles are formed, without any specific nanoscale morphology (data not shown). The results show that application of an electric potential is essential for the formation of CH–Fe_3O_4/ITO nanostructure. It may be noted that the pre-eminent morphology is known to be dependent on the applied potential. However, this voltage-dependence implies that the formation of CH nanostructure requires extra energy. We propose that the extra energy facilitates configurations with induced alignment and uniformity, which is originally restricted to a layered molecular structure bound by the intra and intermolecular hydrogen bonds (Okuyama et al., 1997).

2.4. Functionalization of probe DNA onto electrochemically fabricated CH–Fe_3O_4/ITO electrode

DNA solutions are prepared in tris-EDTA buffer. After electrodeposition, biotin labeled DNA is immobilized onto CH–Fe_3O_4/ITO nano-composite electrode using avidin as a cross-linker under optimized conditions with gentle shaking. 10 μL of avidin (1 mg/mL)

Table 1b
Matched and mismatched duplex DNA used for immobilization onto the electrode.

1+2	1+3	1+4	1+5	1+6	1+7
Matched	(C-T) 6	(A-C) 10	(C-T, C-A) 6, 14	(T-G, A-C) 4, 10	(C-T, A-C) 6, 10

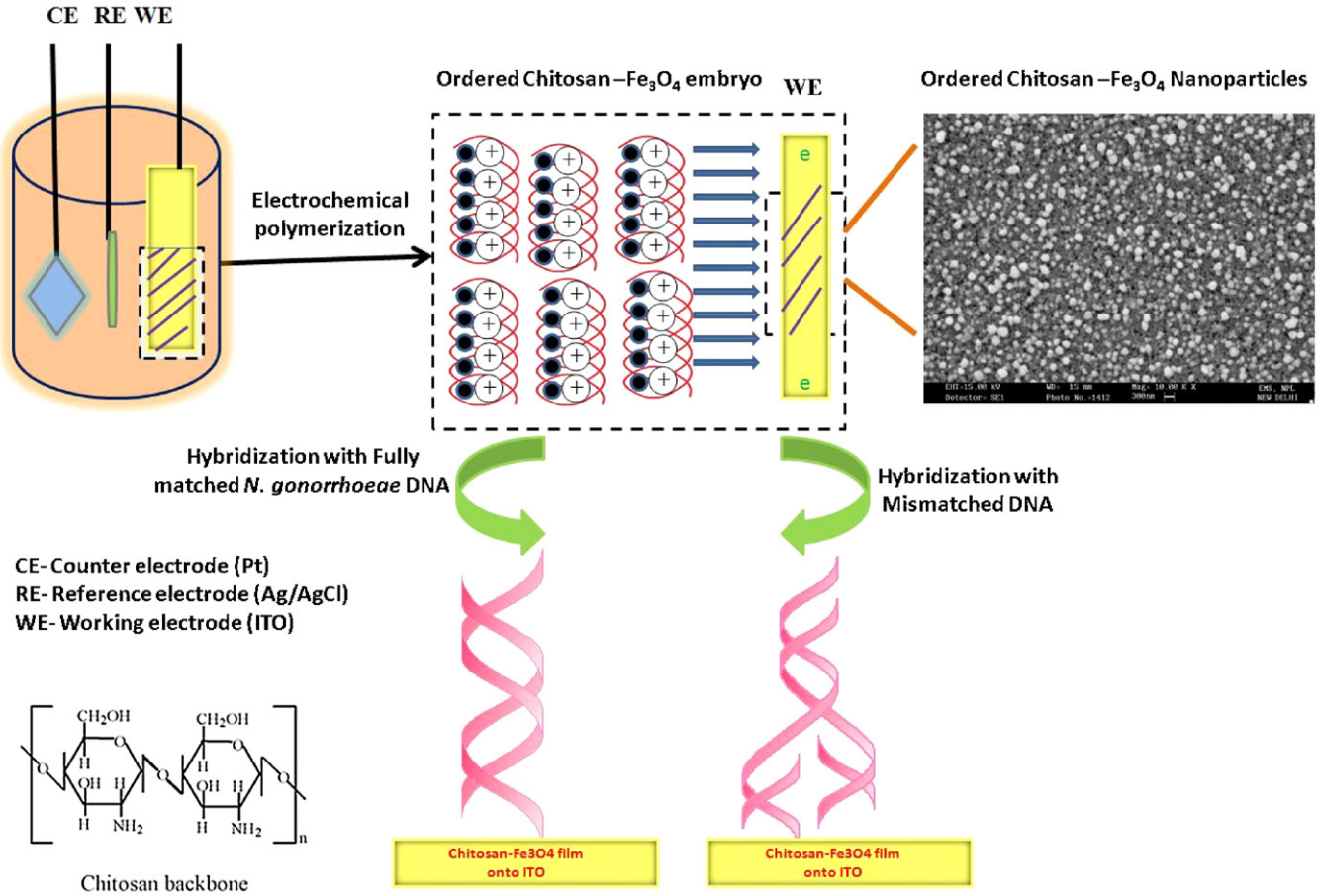

Scheme 1. Schematic representation of electrochemical deposition of highly ordered CH–Fe_3O_4/ITO nano-composite and application of electrochemically fabricated *N. gonorrhoeae* DNA-immobilized electrode for rapid and mismatch-discriminating DNA hybridization.

(activated using 15 mM EDC and 30 mM NHS for 2 h at 25 °C) is immobilized onto CH–Fe_3O_4/ITO nano-composite surface. Avi/CH–Fe_3O_4/ITO electrode is then washed with autoclaved Millipore water and is subject to 5 min incubation with 10 μL of 20-mer biotinylated oligonucleotide probe (1.0 μM) in a humid chamber at 25 °C (Scheme 1 and Supplementary data). The BDNA-Avi/CH–Fe_3O_4/ITO bioelectrode is hybridized with complementary target oligonucleotide for about 60 s at 25 °C.

3. Results and discussion

3.1. Fourier transform infrared (FTIR) and atomic force microscopy (AFM) analysis

The FTIR spectra (Fig. 1a) of pure CH/ITO (curve i) displays all the IR bands corresponding to functional groups present in pure CH (Tian et al., 2003). The IR bands corresponding to –NH and OH stretching modes are shifted to the lower wave number in the IR spectra of CH–Fe_3O_4/ITO nano-composite film (curve ii), corresponding to pure CH. This indicates that amine group of CH is involved in assembling of the Fe_3O_4 nanoparticles. The absorption band of Fe_3O_4 nanoparticles appears at 582 cm^{-1} arising due to both the stretching vibration mode and tensional vibration mode of Fe–O bond in the tetrahedral and in the octahedral sites. The FTIR spectra of Avi/CH–Fe_3O_4/ITO bioelectrode (curve iii) show characteristic peaks at 1565 and 1658 cm^{-1} that are attributed to primary and secondary amide linkages of avidin molecules. In the FTIR spectrum of BDNA/Avi/CH–Fe_3O_4/ITO bioelectrode, vibration bands observed at 1067 and 1243 cm^{-1} are due to the asymmetric stretching of P–O–C vibration and stretching vibration of P=O of the phosphoric acid group, respectively. Peaks seen at 1492 and 1606 cm^{-1} are associated with carbonyl stretching vibration and C=C bonds in the purine and pyrimidine rings (curve iv) (Singh et al., 2009).

Fig. 1b presents the typical AFM images of an electrochemically deposited CH/ITO film (i), CH–Fe_3O_4/ITO nano-composite (ii) and BDNA-Avi/CH–Fe_3O_4/ITO bioelectrode (iii). The AFM studies reveal that Fe_3O_4 nanoparticles are inter-connected by dipole–dipole interactions in the film. The nanoporous rough morphology is observed for CH film and surface roughness of CH film is estimated to be ~19.2 nm (Fig. 1b(i)). The CH–Fe_3O_4 film shows globular nanoporous rough morphology. It appears that Fe_3O_4 nanoparticles are regularly dispersed in the CH film and strongly adhere onto the substrate with porous morphology (Fig. 1b(ii)). The surface roughness of CH–Fe_3O_4 nano-biocomposite increases to ~25.4 nm. Such nanoporous rough morphology results in increased effective surface area of the substrate electrode to load large amount of DNA, and may perhaps prevent the leaching of DNA molecules from the biosensor surface. The surface roughness of BDNA-Avi/CH–Fe_3O_4/ITO bioelectrode decreases to ~5.44 nm indicating immobilization of the biotinylated DNA. When DNA is entrapped in this network-like film, aggregates of the DNA molecules exhibit island-like structures (Fig. 1b(iii)) that may facilitate specific reaction between substrate and DNA, resulting in enhanced amperometric response of the biosensor (Li et al., 2000). Results obtained by AFM studies are well correlated with those of the SEM studies (Supplementary fig. 1c).

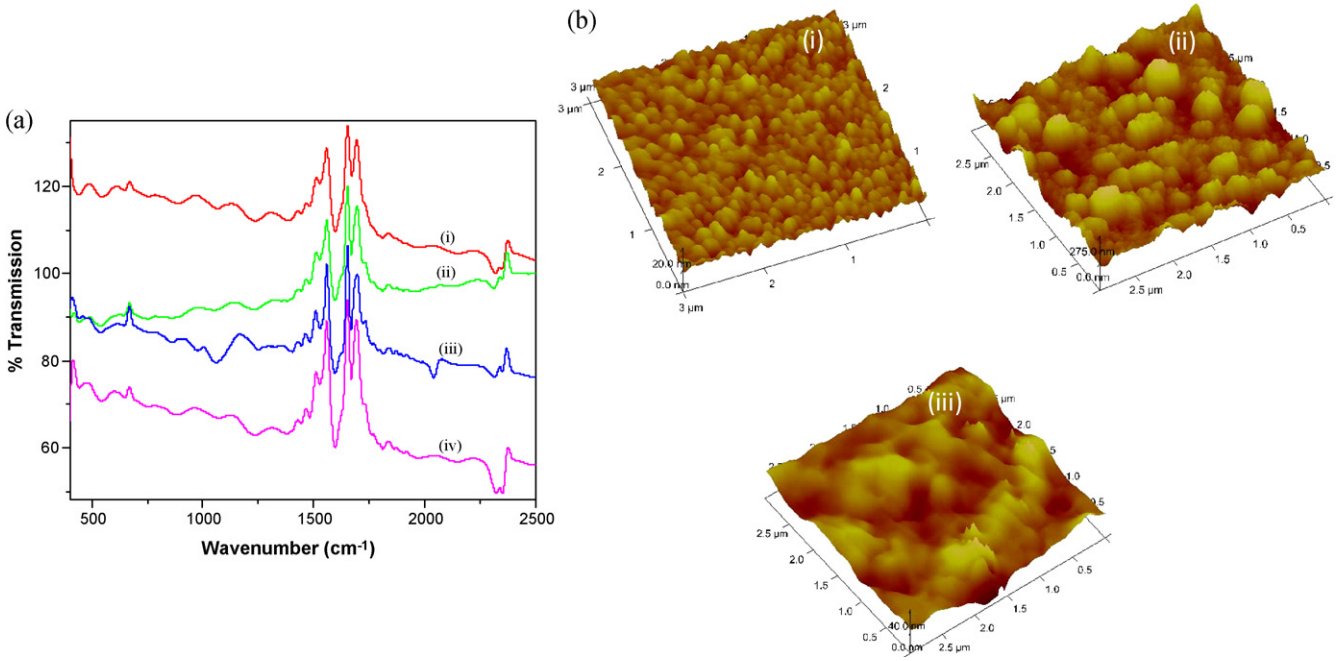

Fig. 1. (a) FT-IR spectra of (i) CH/ITO, (ii) CH–Fe_3O_4/ITO, (iii) Avi/CH–Fe_3O_4/ITO, and (iv) BDNA/Avi/CH–Fe_3O_4/ITO electrodes and (b) AFM images of (i) CH/ITO, (ii) CH–Fe_3O_4/ITO, and (iii) BDNA/Avi/CH–Fe_3O_4/ITO electrodes.

3.2. Optimization of deposition potential

CH/ITO and CH–Fe_3O_4/ITO nano-composite films have been prepared electrochemically in the potential range, −0.5 V to −2.5 V. In the case of CH/ITO (Fig. 2a), we observe variation in the peak current and shift in the peak (Fig. 2a) with applied potential. However, in the case of CH–Fe_3O_4/ITO (Fig. 2b) electrode, there is a negligible shift in the peak of CH–Fe_3O_4/ITO CV at various applied potentials. On inclusion of the Fe_3O_4 nanoparticles the film is found to be stable. It can be concluded that −1.0 V is the appropriate potential for the fabrication of the CH–Fe_3O_4 film onto ITO plate since it yields higher peak current. The insets (Fig. 2a and b) show the various chrono-amperometric curves obtained for CH/ITO and CH–Fe_3O_4/ITO nano-composite films, respectively.

3.3. Electrochemical impedance spectroscopy (EIS)

Fig. 2c shows the results of the EIS measurements carried out as a function of frequency on an electrochemically deposited CH/ITO film (i), CH–Fe_3O_4/ITO nano-composite (ii), an Avi/CH–Fe_3O_4/ITO (iii), and a BDNA-Avi/CH–Fe_3O_4/ITO bioelectrode (iv) in 0.05 M phosphate buffer saline (PBS) of pH 7.0 containing 5 mM $[Fe(CN)_6]^{3-/4-}$. The charge transfer resistance (R_{et}) of CH–Fe_3O_4/ITO electrode (curve ii) is found to decrease to 2.75 kΩ with respect to the CH/ITO electrode ($R_{et} \sim 5.81$ kΩ, curve i) and the lower value of R_{et} of CH–Fe_3O_4/ITO electrode reveals nanosized structure of Fe_3O_4 particles that provide increased electroactive surface leading a higher rate of electron transfer. However, when biotinylated ssDNA is immobilized onto CH–Fe_3O_4/ITO electrode, R_{et} of the electrode increases to 4.18 kΩ assigned to the presence of electro-negative phosphate skeleton that perhaps prevent $[Fe(CN)_6]^{3-/4-}$ ions from reaching the electrode surface for electron transfer during redox reaction. This implies that BDNA is successfully immobilized onto the electrochemically prepared nanostructured CH–Fe_3O_4/ITO electrode (curve iv).

3.4. Cyclic voltammetry (CV)

Fig. 2d shows the results of the CV measurements carried out on an electrochemically deposited CH/ITO film (i), CH–Fe_3O_4/ITO nano-composite (ii), an Avi/CH–Fe_3O_4/ITO (iii), and a BDNA-Avi/CH–Fe_3O_4/ITO bioelectrode (iv) in 0.05 M PBS of pH 7.0 containing 5 mM $[Fe(CN)_6]^{3-/4-}$ at a scan rate of 50 mV/s, respectively. The CV of pure CH electrode (curve i) shows well-defined cathodic peak at −0.0137 V and an anodic peak at 0.260 V in the potential range of 0.6 to −0.30 V having peak current of 151 μA. However, significant change (curve ii) in peak potential [cathodic peak potential (E_{pc}) to −0.0346 V and anodic peak potential (E_{pa}) to 0.295] with increased peak current of 238 μA is observed on inclusion of Fe_3O_4 nanoparticles. This may be attributed to the presence of Fe_3O_4 nanoparticles with increased mobility resulting in enhanced adsorption of the redox moieties on cationic CH–Fe_3O_4/ITO nano-composite surface with improvement in electron transfer and electrical conductivity. It can be seen that there is considerable decrease in the intensity of these redox peaks after the immobilization of avidin indicating the binding of avidin onto CH–Fe_3O_4/ITO surface as a cross-linker (curve iii). Further, the observed enhancement in the redox peak can be attributed to binding of BDNA onto CH–Fe_3O_4/ITO surface in agreement with literature (curve iv) (Arora et al., 2007; Jiang and Wang, 2001). The surface concentration value of redox species of electrolyte [Fe(III)/Fe(IV)] onto CH–Fe_3O_4/ITO electrode has been found to be 0.437×10^{-6} mol cm^{-2}. The total surface concentration of redox species of electrolyte [Fe(III)/Fe(IV)] is found to be 7.97×10^{-7} mol cm^{-2} indicating improved immobilization of BDNA onto Avi/CH–Fe_3O_4/ITO electrode indicating BDNA-Avi/CH–Fe_3O_4/ITO to be a promising matrix for the fabrication of STD biosensor (Supplementary fig. 2a,b).

3.5. Biosensing characteristics of BDNA/Avi/CH–Fe_3O_4/ITO bioelectrode with patient samples

The BDNA/Avi/CH–Fe_3O_4/ITO STD sensor has been used to detect sequence specific DNA based on the DPV current change

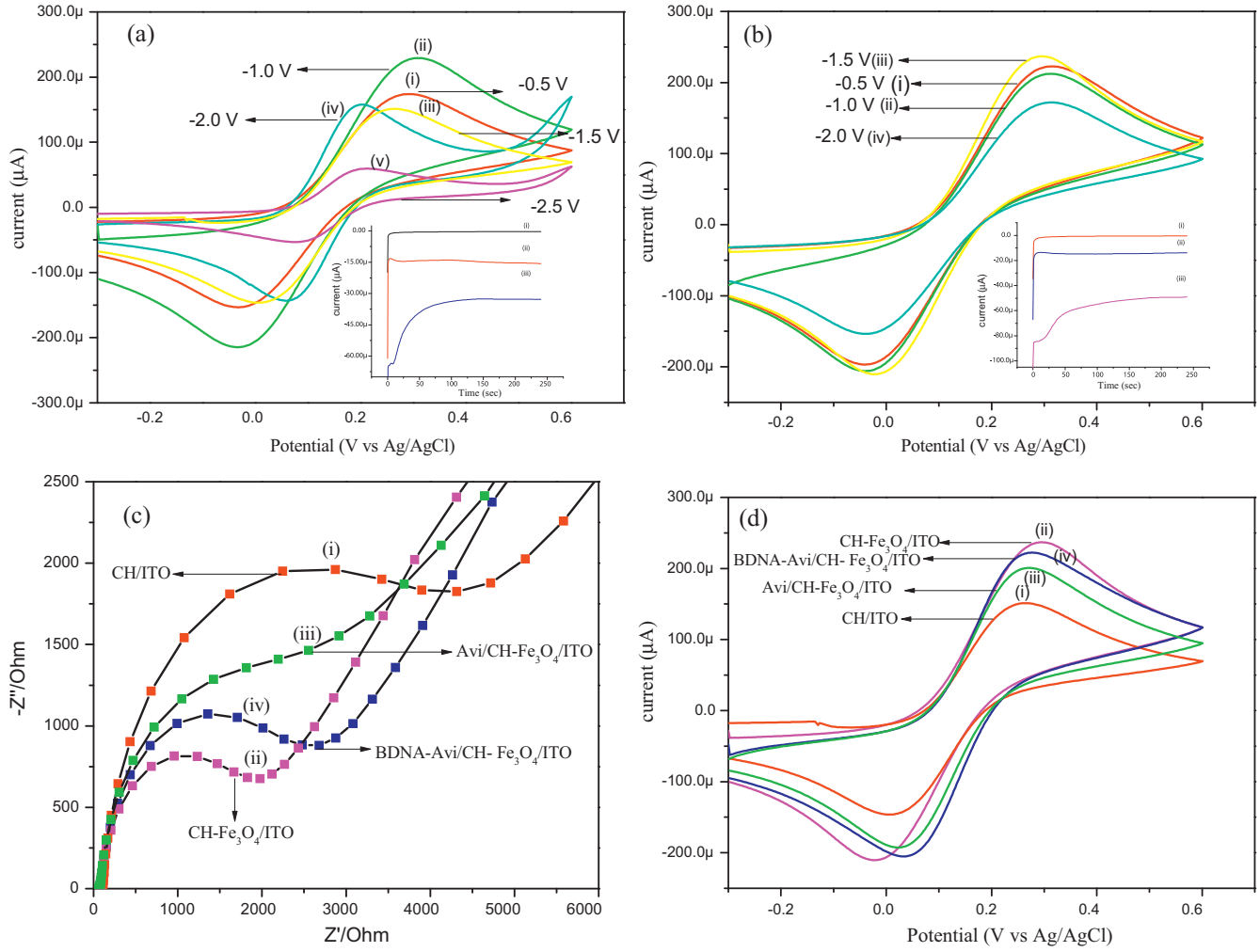

Fig. 2. (a) CV of CH/ITO at different potentials (i) 0.5 V, (ii) 1.0 V, (iii) 1.5 V, (iv) 2.0 V, and (v) 2.5 V (inset shows chronoamperometric curve); (b) CV of CH–Fe_3O_4/ITO at different potentials (i) 0.5 V, (ii) 1.0 V, (iii) 1.5 V, (iv) 2.0 V, and (v) 2.5 V (inset shows chronoamperometric curve); (c) EIS curve of (i) CH/ITO, (ii) CH–Fe_3O_4/ITO, (iii) Avi/CH–Fe_3O_4/ITO, and (iv) BDNA/Avi/CH–Fe_3O_4/ITO bioelectrodes; and (d) CV of (i) CH/ITO, (ii) CH–Fe_3O_4/ITO, (iii) Avi/CH–Fe_3O_4/ITO, and (iv) BDNA/Avi/CH–Fe_3O_4/ITO bioelectrodes in 0.05 M PBS containing 5 mM $[Fe(CN)6]^{3-/4-}$.

of MB before and after hybridization (Kerman et al., 2002; Erdem et al., 2000). Fig. 3a shows DPV response of the fabricated STD bioelectrode. The performance of the BDNA/Avi/CH–Fe_3O_4/ITO electrode has been studied by incubating with DNA extracted from *N. gonorrhoeae* culture isolated sample, pus sample spiked with *N. gonorrhoeae* and *N. gonorrhoeae* positive male patient sample (see Supplementary data). The observed significant decrease in the DPV signal shows that the complementary DNA present in the clinical sample hybridizes with the probe DNA (Fig. 3a). The observed minor variation in DPV signal can be assigned to sample-to-sample variation arising due to varying bacterial DNA load that cannot be quantified (Ansari et al., 2009; Singh et al., 2010; Wang, 2000; Wang et al., 2002).

Fig. 3b shows the results of response studies carried out with respect to the concentration of target DNA sequence with BDNA/Avi/CH–Fe_3O_4/ITO electrode using MB as redox indicator. The observed peak current for the reduction of MB after hybridization with cDNA decreases with the target concentration up to 1×10^{-6} M, and remains constant with further increase in the target concentration indicating that all the immobilized probe molecules on the bioelectrode surface are involved in hybridization at concentration of 1×10^{-6} M. Prior to this threshold concentration, MB reduction signal decreases with increased target concentration that perhaps prevents interaction of guanine molecules with MB due to the duplex formation. The observed constant MB signal reveals that all the hybridization sites on BDNA/Avi/CH–Fe_3O_4/ITO electrode are covered. The change in peak current of MB is linearly related to log (concentration) of cDNA between 1×10^{-6} M and 1×10^{-16} M. The detection limit of BDNA/Avi/CH–Fe_3O_4/ITO is 1.0×10^{-15} M (calculated from blank signal). It is found that decrease in the MB peak current (I Target) with respect to cDNA concentration (Fig. 3b inset) follows Eq. (1) with value of regression co-efficient as 0.99.

$$\text{I Target} = 2.67818\,[\log(\text{Target concentration})] + 13.92 \quad (1)$$

The experiments have been repeated at least 15 times and the error bars are included in Fig. 3b.

Sensor regeneration is critical in order to ascertain that a signal arises due to the specific interactions with the target and is not due to some other non-specific modification of the probe or sensor head. The background current has been measured using DPV. The sensors have been challenged with 1 μM target to determine signal suppression. It is found that the sensor is stable enough to allow for ready regeneration: a low ionic strength short wash (30 s at room temperature (25 °C) autoclaved distilled water (~18.2 MΩ)) (Fig. 3c) (Lubin et al., 2006) is sufficient to recover the original sensor signal and it is found that this sensor can be used at least for 6–8 times before significant degradation is observed. For storage, sensors have been fabricated, tested, and regenerated as above.

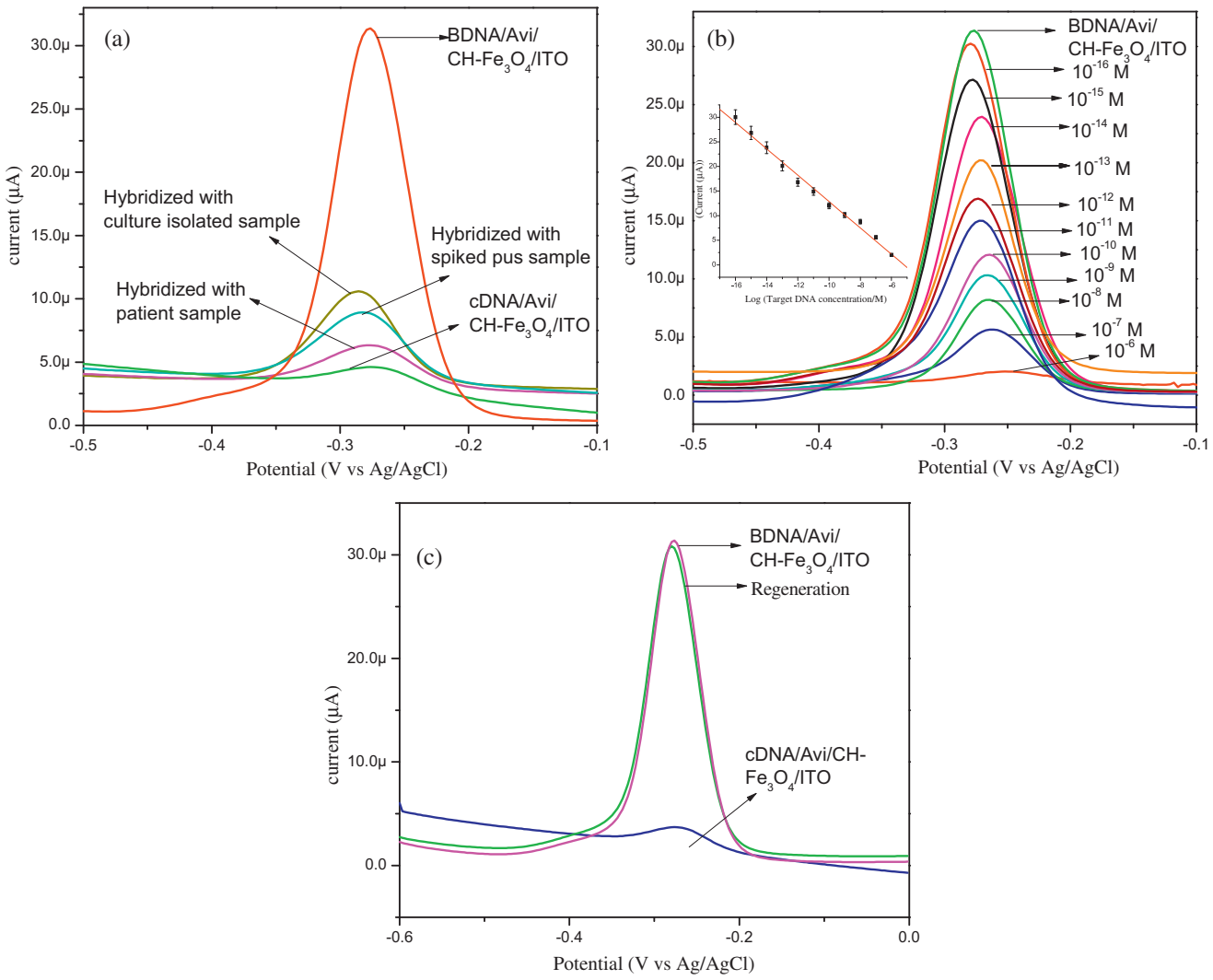

Fig. 3. (a) DPVs of BDNA/Avi/CH–Fe_3O_4/ITO bioelectrode to detect the presence of complementary target sequence in *N. gonorrhoeae* clinical samples; culture isolated, spiked pus, patient samples, artificial complementary DNA. (b) DPV of BDNA/Avi/CH–Fe_3O_4/ITO after hybridization with cDNA concentration 1×10^{-16}–1×10^{-6} M DNA at step potential of 3 mV and modulation amplitude of 50 mV in 20 μM MB, pretreatment at +0.1 V for 10 s, 0.05 M PBS (pH 7.0, 0.9% NaCl) (inset shows the MB peak height as a function of cDNA concentration). (c) The regeneration of sensor: the sensor in which the addition of a complementary target strand results in a decrease in measured current. Because all of the sensing components are strongly adsorbed to the sensor surface, the sensor is readily regenerated with a 30 s distilled water rinse, as shown.

In addition, the electrode can be stored for more than 6 months at 4 °C without significant loss in their activity for hybridization and are thus suited for a stable platform for further quantitative measurements.

3.6. Mismatch discriminating DNA hybridization

The ability to discern base mismatch is an important characteristic of a DNA biosensor. The specificity of the biosensor has been investigated using BDNA-Avi/CH–Fe_3O_4/ITO electrode to hybridize with different target ssDNA (one and two-base mismatches) sequences (Fig. 4a). The results are summarized in Table 1c. To evaluate the effect of different mismatches by DPV, we have used five different ssDNA target sequences (Table 1a). The ssDNA target (C-T) contains base T instead of base G at 6th position. The ssDNA target (A-C) contains base C instead of base T at the 10th position. The ssDNA target having two-base mismatch is (C-T, C-A), (T-G, A-C), (C-T, A-C) at position (6, 14), (4, 10,), (6, 10), respectively. Fig. 4a shows the variation of the peak current obtained using DPV measurements after incubating the sensor with equivalent amount of targets each having a single base-pair mismatch, in relation to the immobilized BDNA probe. As expected, the lowest peak current is observed if the target is fully complementary to the immobilized BDNA probe (Fig. 4a). A significant percentage (%) decrease in current (I_{pa}) to 80% is observed after BDNA-Avi/CH–Fe_3O_4/ITO electrode hybridized with cDNA indicates the successful hybridization. And when the single mismatched base (C-T) is at the 6th position the % decrease in I_{pa} is about 40%. When the single mismatched base (A-C) is at the 10th position, % decrease in I_{pa} is almost 57%. The contribution of a mismatch to DNA duplex stability depends on the location of the mismatch, its nearest neighbors and its orientation. As both the A-C and C-T mismatches are present internally and

Table 1c
Percentage (%) decrease in hybridization events between the BDNA-Avi/CH–Fe_3O_4/ITO electrode and different base mismatch DNA sequences.

Target DNA	I_{pa} of MB (μA)	% decrease in I_{pa}
No target DNA (only probe)	30	0
cDNA	6	80
OBM1 (C-T) 6th position	18	40
OBM2 (A-C) 10th position	13	57
TBM1 (C-T, C-A) 6th and 14th position	28	6.7
TBM2 (T-G, A-C) 4th and 10th position	21	30
TBM3 (C-T, A-C) 6th and 10th position	19	37

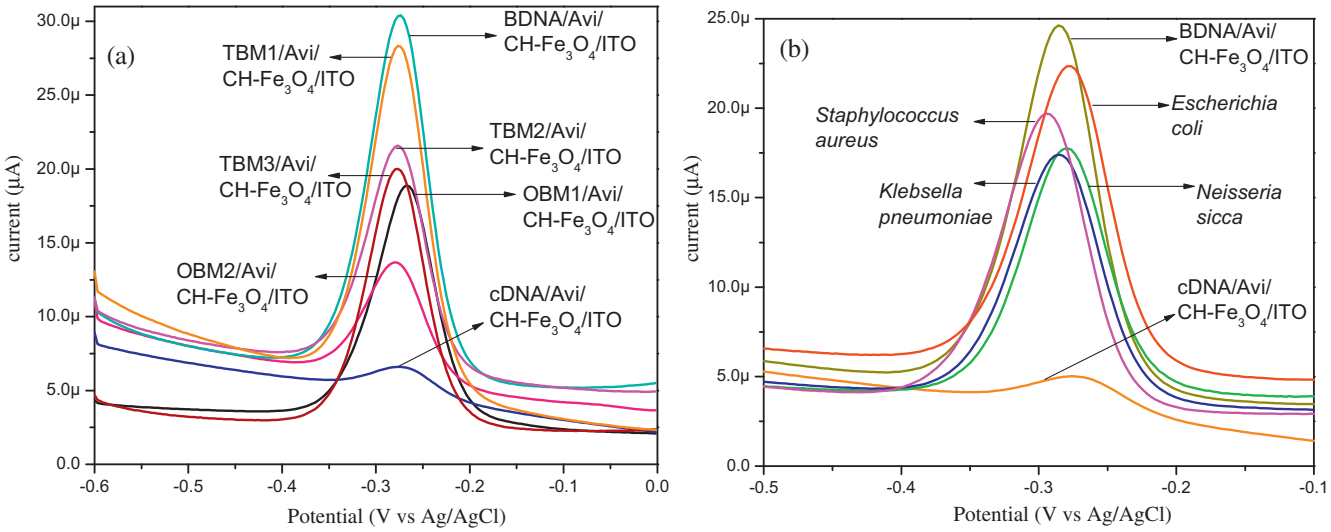

Fig. 4. (a) DPVs of BDNA/Avi/CH–Fe_3O_4/ITO bioelectrode to detect one and two-base mismatch-discriminating DNA hybridization. (b) DPVs of BDNA/Avi/CH–Fe_3O_4/ITO bioelectrodes to detect the presence of non-complementary target sequence in other NgNs and other GNBs at step potential of 3 mV and modulation amplitude of 50 mV in 20 M MB, pretreatment at +0.1 V for 10 s, 0.05 M PBS (pH 7.0, 0.9% NaCl).

stability of C-T and A-C mismatch is almost equivalent, difference in the peak may be attributed to the presence of G**T**T, A**C**G bases adjacent to the mismatch, respectively. These factors determine the free energy change of the hybridization reaction. Similarly, the % decrease in I_{pa} is evaluated with two mismatched bases at different points in the DNA sequence. It may be noted that when both the mismatches are at the two ends of the sequence; (C-T, C-A), i.e., at the 6th position and 14th position, the % decrease in I_{pa} is about 6.7% and the peak current is higher, indicating non-hybridization. With two base mismatches (T-G, A-C), i.e., at the 4th position and 10th position, the % decrease in I_{pa} is about 30%. With two base mismatches (C-T, A-C), i.e., at the 6th position and 10th position, the % decrease in I_{pa} is about 37%. It may be noted that the reduction peak current of the STD biosensor in the presence of cDNA is higher than that of the biosensor in the presence of one-base mismatch and two-base mismatch target DNA. Such difference may originate from the varied binding affinity of MB with cDNA, one-base mismatch and two-base mismatch target DNA. The peak current from a competitive DPV experiment is found to be reproducible and can be quantified for even a single base-pair mismatch detection.

3.7. Specificity test with non-Neisseria gonorrhoeae Neisseria species and other gram negative bacteria

Fig. 4b shows DPV response of the STD sensor to cultures of *Escherichia coli*, *Neisseria sicca*, *Staphylococcus aureus* and *Klebseilla pneumoniae*. The specificity of the bioelectrode has been studied by incubating the probe electrode with DNA extracted from other non-*Neisseria gonorrhoeae Neisseria* species (NgNs) as well as other gram negative bacteria (GNBs). No significant decrease in the signal is obtained in the presence of *E. coli*, *N. sicca*, *S. aureus* and *K. pneumoniae* DNA indicating the specificity of probe DNA for *N. gonorrhoeae* detection.

4. Conclusions

We have demonstrated a simple, convenient electrochemical approach to fabricate CH–Fe_3O_4/ITO nanostructured platform for biosensor application. The electrochemistry has been investigated of probe DNA immobilized onto CH–Fe_3O_4/ITO matrix containing both fully matched and mismatched DNA using MB as a redox indicator. The BDNA-Avi/CH–Fe_3O_4/ITO electrode provides discrimination between cDNA, one and two-base mismatches out of 20 bases in a targeted attachment region having detection limit (1×10^{-15} M) in a wide dynamic range (from 1×10^{-16} M to 1×10^{-6} M). When the mismatch is at two ends of the sequence; (C-T, C-A), i.e., at the 6th position and 14th position the % decrease in I_{pa} is very negligible about 6.7% indicating non-hybridization. The combination of excellent immobilization of DNA, high conductivity and the advantages of metal nanoparticles in the electron transfer, enhance the specificity and sensitivity of the biosensor. The bioelectrode demonstrates a high degree of accuracy for the detection of *N. gonorrhoeae* nucleic acid with substantial minimization or virtual elimination of false positive readings as this assay has the capability of detecting even a single base mismatch in the target DNA. Electrochemical DNA sensors have the potential to meet the need for inexpensive, rapid and hand-held detection systems. Efforts are being made to destabilize the duplex formation under stringent conditions to improve the mismatch discrimination. Further, studies should be carried out to explain difference in peaks based on the thermodynamics of the mismatch sequences.

Acknowledgements

The authors thank Prof. R.C. Budhani, Director, National Physical Laboratory, New Delhi, India for the facilities. Renu Singh is thankful to Council of Scientific and Industrial Research (CSIR), India for the award of Senior Research Fellowship. The authors thank Dr. K.N. Sood, Mr. S.B. Samanta and Mr. Sandeep Singh for providing the required facilities for SEM and AFM analysis, respectively. We thank Dr. V.K. Sharma, Professor and Head, Dermatology, AIIMS, Dr. J.C. Samantaray, Professor and Head and Dr. Arti Kapil, Professor, Microbiology, AIIMS, Dr. Manju Bala, Senior Microbiologist, Safdarjang Hospital, New Delhi for useful discussions. We acknowledge financial support received from the Department of Science & Technology (DST) [DST/TSG/ME/2008/18 and GAP-070932], in-house project (OLP-070632D) and Department of Biotechnology, Govt. of India (DBT/GAP070832).

Appendix A. Supplementary data

Supplementary data associated with this article can be found, in the online version, at doi:10.1016/j.bios.2010.11.047.

References

Ansari, A.A., Singh, R., Sumana, G., Malhotra, B.D., 2009. Analyst 134, 997.
Arora, K., Prabhakar, N., Chand, S., Malhotra, B.D., 2007. Anal. Chem. 79, 6152–6158.
Cao, D.F., He, P.L., Hu, N.F., 2003. Analyst 128, 1268.
Erdem, A., Kerman, K., Meric, B., Akarca, U.S., Ozsoz, M., 2000. Anal. Chim. Acta 422, 139.
Gong, P., Li, H., He, X., Wang, K., Hu, J., Tan, W., Zhang, S., Yang, X., 2007. Nanotechnology 18, 7.
Guo, L., Pei, G.L., Wang, T.J., Ang, Z.W., Jin, Y., 2007. Colloids Surf. A: Physicochem. Eng. Asp. 293, 58.
Huang, M.H., Bi, L.H., Shen, Y., Liu, B.F., Dong, S.J., 2004. J. Phys. Chem. B 108, 9780.
Iida, H., Takayanagi, K., Nakanishi, T., Osaka, T., 2007. J. Colloid Interface Sci. 314, 274.
Jiang, M., Wang, J.J., 2001. Electroanal. Chem. 500, 584.
Katz, E., Weizmann, Y., Willner, I., 2005. J. Am. Chem. Soc. 127, 9191.
Kaushik, A., Khan, R., Solanki, P.R., Pandey, P., Alam, J., Ahmad, S., Malhotra, B.D., 2008. Biosens. Bioelectron. 24, 676.
Kerman, K., Ozkan, D., Kara, P., Meric, B., Gooding, J.J., Ozsoz, M., 2002. Anal. Chim. Acta 462, 39–47.
Lee, D.K., Kim, Y.H., Kim, C.W., Cha, H.G., Kang, Y.S., 2007. J. Phys. Chem. B 111, 9288.
Li, C.N., Djuris, A.B., Kwong, C.Y., Lai, P.T., Chan, W.K., Liu, S.Y., 2005. Appl. Phys. A: Mater. Sci. Process. 80, 301.
Li, J., Piehler, L.T., Qin, D., Baker, J.R., Tomalia Jr., D.A., 2000. Langmuir 16, 5613.
Loh, K., Lee, Y.H., Musa, A., Salmah, A.A., Zamri, I., 2008. Sensors 8, 5775.
Lubin, A.A., Lai, R.Y., Baker, B.R., Heeger, A.J., Plaxco, K.W., 2006. Anal. Chem. 78, 5671.
Mukenge-Tshibaka, L., Alary, M., Bernier, F., van Dyck, E., Lowndes, C.M., Guédou, A., Anagonou, S., Joly, J.R., 2000. J. Clin. Microbiol. 38, 4076.
Okuyama, K., Noguchi, K., Miyazawa, T., Yui, T., Ogawa, K., 1997. Macromolecules 30, 5849.
Peppas, N.A., Hilt, J.Z., Khademhosseini, A., Langer, R., 2006. Adv. Mater. 18, 1345.
Singh, R., Dhand, C., Sumana, G., Verma, R., Sood, S., Gupta, R.K., Malhotra, B.D., 2010. J. Mol. Recognit. 23, 472.
Singh, R., Prasad, R., Sumana, G., Arora, K., Sood, S., Gupta, R.K., Malhotra, B.D., 2009. Biosens. Bioelectron. 24, 2232.
Smith, D.W., Tapsall, J.W., Lum, G., 2005. Commun. Dis. Intell. 29, 358.
Tabrizi, S.N., Chen, S., Cohenford, M.A., 2004. Sex. Transm. Infect. 80, 68.
Tian, F., Liu, Y., Hu, K., Zhao, B., 2003. J. Mater. Sci. 38, 4709.
Tripathy, D., Adeyeye, A.O., 2005. Proceedings of 5th IEEE Conference on Nanotechnology.
Wang, J., 2000. Nucleic Acid Res. 28, 3011.
Wang, J., Xu, D., Polsky, R., 2002. J. Am. Chem. Soc. 124, 4208.
Whitehead, R.N., Overton T.W., Snyder, L.A., McGowan, S.J., Smith, H., Cole, J.A., Saunders, N.J., 2007. BMC Genomics, doi:10.1186/1471-2164-8-35.
WHO, 2001. Global Prevalence and Incidence of Selected Curable Sexually Transmitted Infections: Overview and Estimates. World Health Organization, Geneva.